Supporting Information

Dendritic $CuBi_2O_4$ Array Photocathode Coated with Conformal TiO_2 Protection Layer for Efficient and Stable Photoelectrochemical Hydrogen Evolution Reaction

*Qing Zhang, Bowen Zhai, Zheng Lin, Xinqing Zhao, Peng Diao**

School of Materials Science and Engineering, Beihang University, Beijing 100191, P.R.China

* Peng Diao (*pdiao@buaa.edu.cn*); *Tel. & Fax: 86-10-82339562*

Chemical and Materials. Bismuth nitrate pentahydrate ($Bi(NO_3)_2 \cdot 5H_2O$), potassium titanium oxalate ($K_2TiO(C_2O_4)_2$)) were purchased from Shanghai Macklin Biochemical Co., Ltd. Cupric (II) acetate monohydrate ($Cu(OAc)_2 \cdot H_2O$) was purchased from Xilong Scientific Co., Ltd. Ethylene glycol, pure ethanol and methanol were purchased from Beijing Chemical Reagents Company. P-benzoquinone was purchased from Sinopharm Chemical Reagent Co., Ltd. All of these chemicals were analytical reagents and used without further purification. Fluorine-doped tin oxide substrates (FTO) (F: SnO_2, 8.0 $\Omega \cdot sq^{-1}$, transparency 80 %, 2.00 cm×3.00 cm) were purchased from Asahi Glass, Japan.

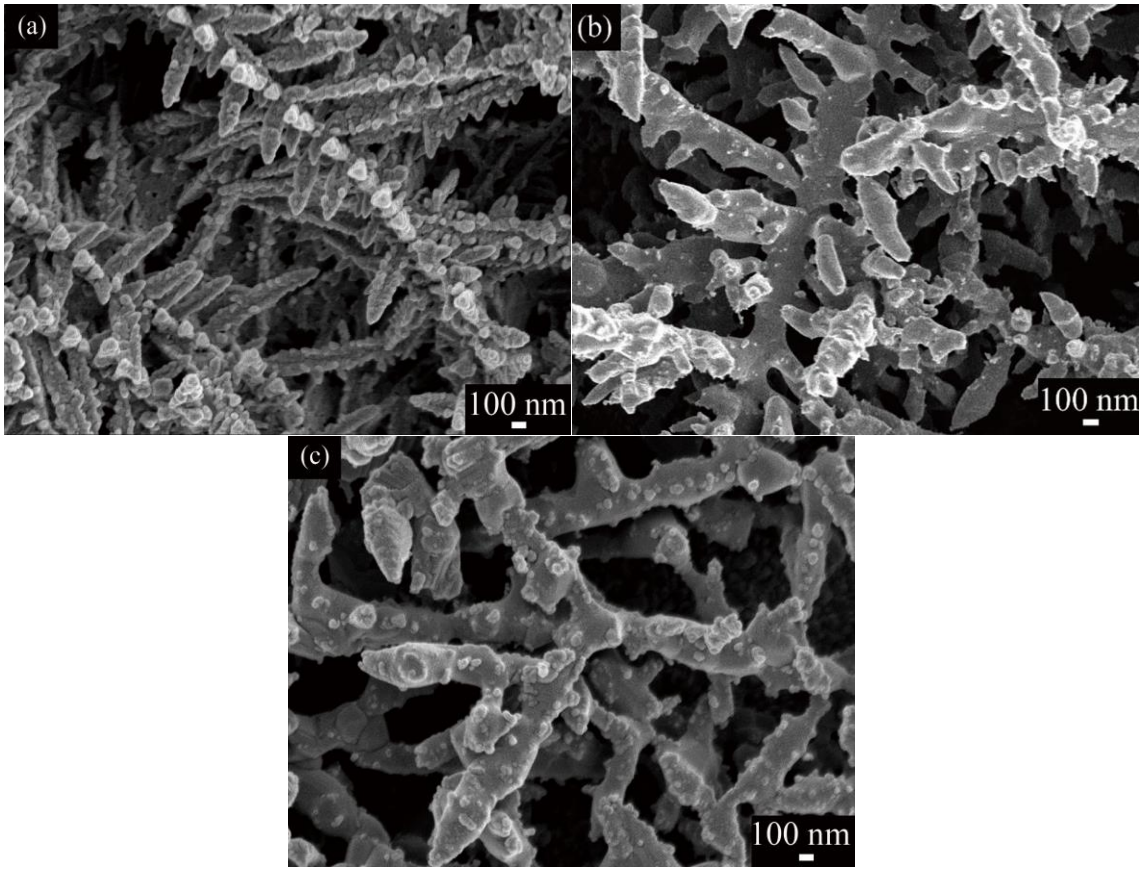

Figure S1. Typical SEM images of the (a) Bi, (b) Bi_2O_3, and (c) $CuBi_2O_4$ dendrites.

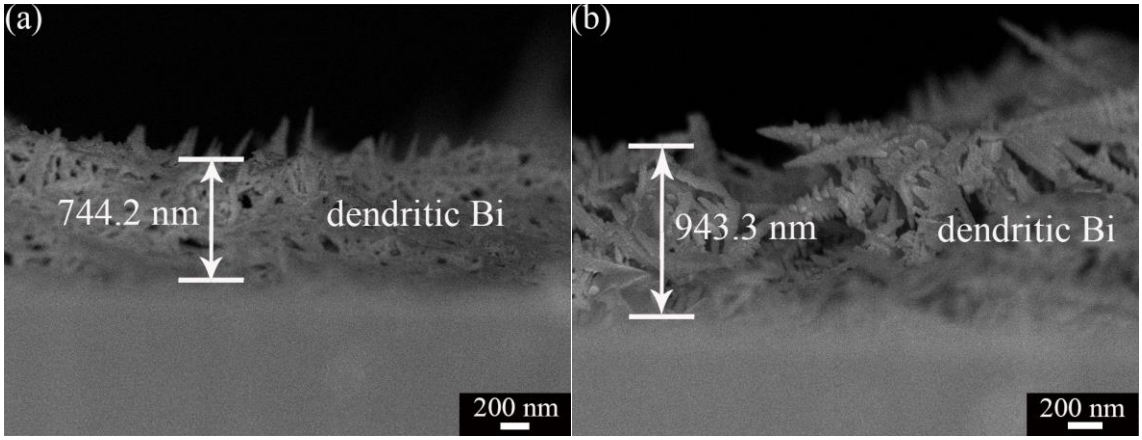

Figure S2. Typical cross-sectional SEM images of the Bi dendrites with the repeated electrodeposition cycle of (a) 16 and (b) 20 times.

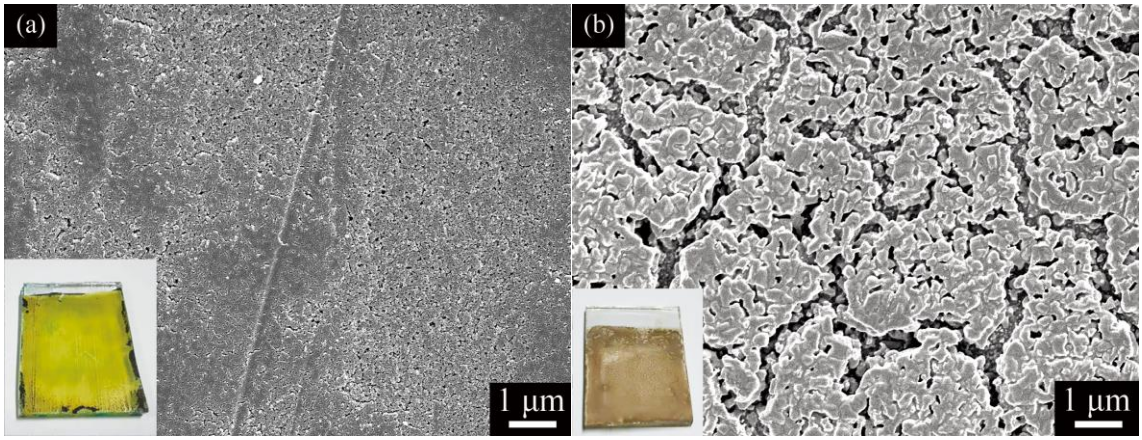

Figure S3. SEM images and optical images (inset) of (a) the Bi film after drop-coating with $Cu(OAc)_2$ methanol solution and drying in air, and (b) the corresponding $CuBi_2O_4$ film after thermal solid state reaction.

The above SEM images clearly shows that, if the metal Bi dendrites were not converted into Bi_2O_3 and were directly drop-coated with $Cu(OAc)_2$ solution, the dendritic structure would no longer existed. In fact, the Bi dendritic structure was destroyed by the dissolution of Bi because Bi could be oxidized by Cu^{2+} due to the following reaction $Bi + Cu^{2+} \rightarrow Bi^{3+} + Cu$.[1] As the released Bi^{3+} ions were ready to form yellow BiOOH via hydrolysis, the yellow film obtained after drop-coating and drying (the inset of **Figure S3a**) confirms the above reactions.

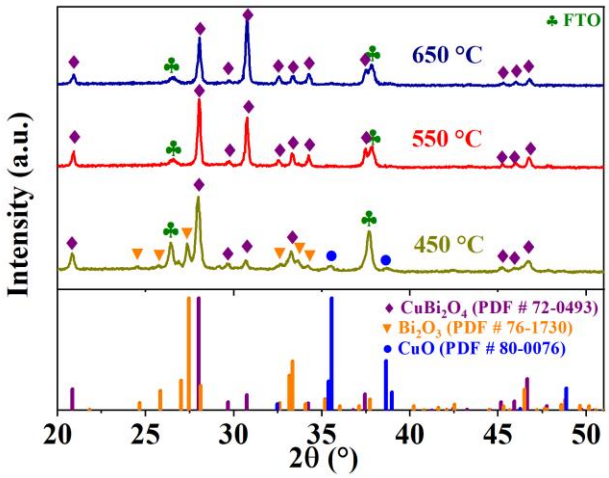

Figure S4. XRD patterns of the $CuBi_2O_4$ dendrites prepared at different temperatures for 2 h: (a) 450 °C, (b) 550 °C, (c) 650 °C.

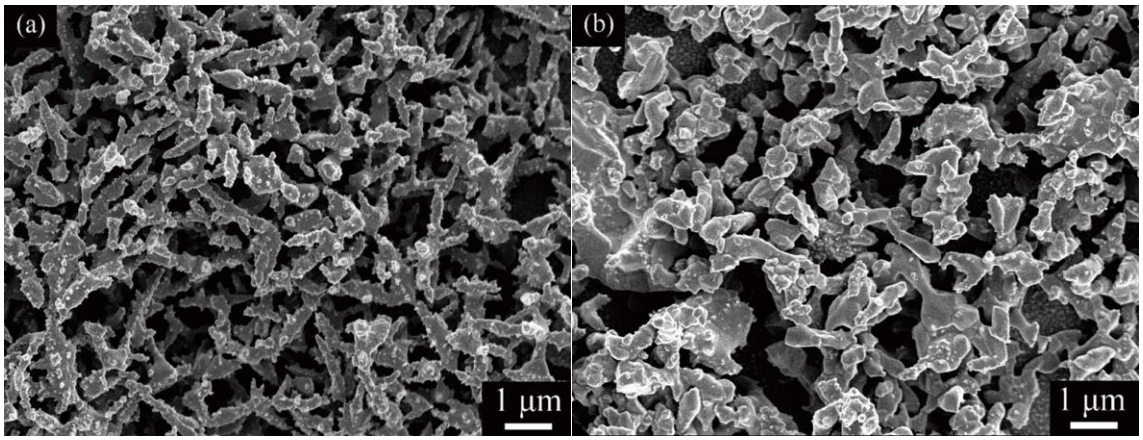

Figure S5. SEM images of the $CuBi_2O_4$ dendrites prepared at different thermal reaction temperatures for 2 h: (a) 450 °C, (b) 650 °C.

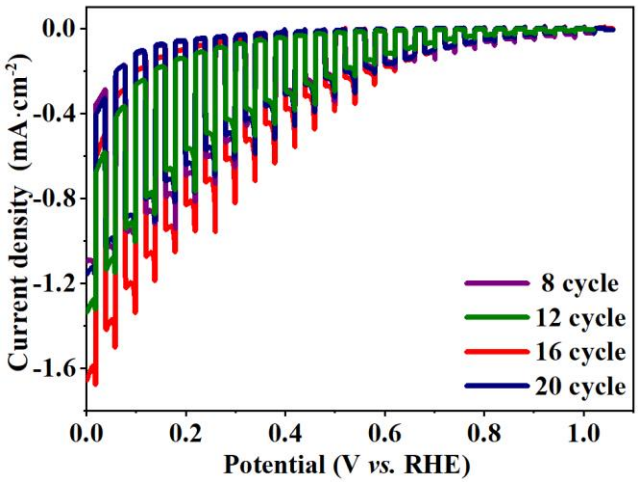

Figure S6. Linear sweep voltammetric curves of the dendritic $CuBi_2O_4$ photocathodes prepared at different repeated cycles during the electrodeposition of Bi dendritic template in 0.10 M Na_2SO_4 solution at a potential sweep rate of 10 mV s^{-1} under chopped illumination (100.0 mW cm^{-2}).

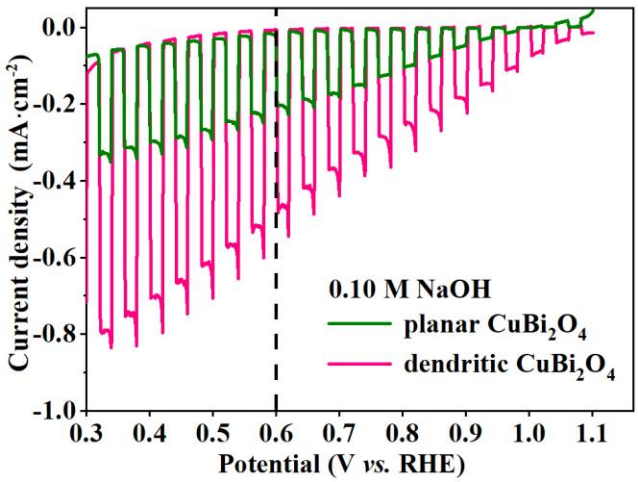

Figure S7. Linear sweep voltammetric curves of the planar and the dendritic $CuBi_2O_4$ photocathodes in 0.10 M NaOH solution at a potential sweep rate of 10 mV s^{-1} under chopped illumination (100.0 mW cm^{-2}).

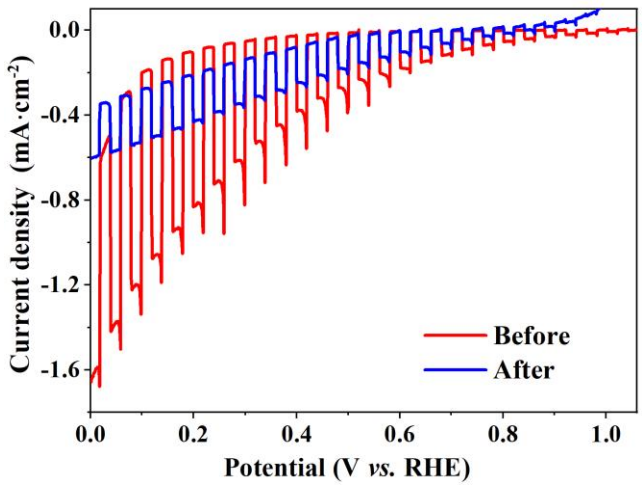

Figure S8. Linear sweep voltammetric curves of the dendritic $CuBi_2O_4$ photocathode before and after PEC HER measurement in 0.10 M Na_2SO_4 at a potential sweep rate of 10 mV s^{-1} under chopped illumination (100.0 mW cm^{-2}). The PEC HER measurements were carried out in 0.10 M Na_2SO_4 at 0.200 V vs. RHE under 100.0 mW cm^{-2} for 1000 s.

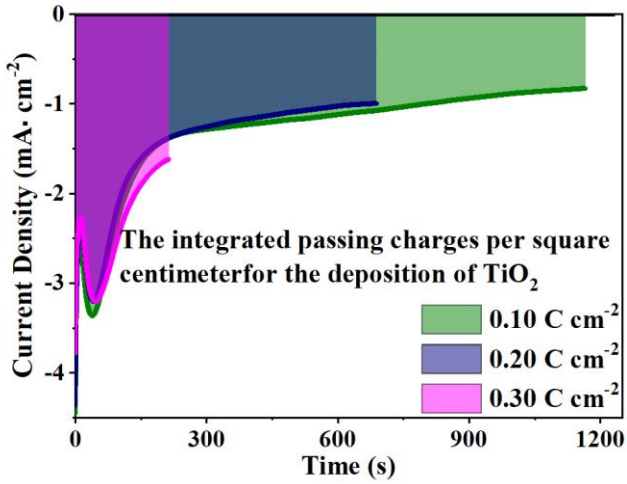

Figure S9. The current density-time response during the electrodeposition of TiO_2 overlayer.

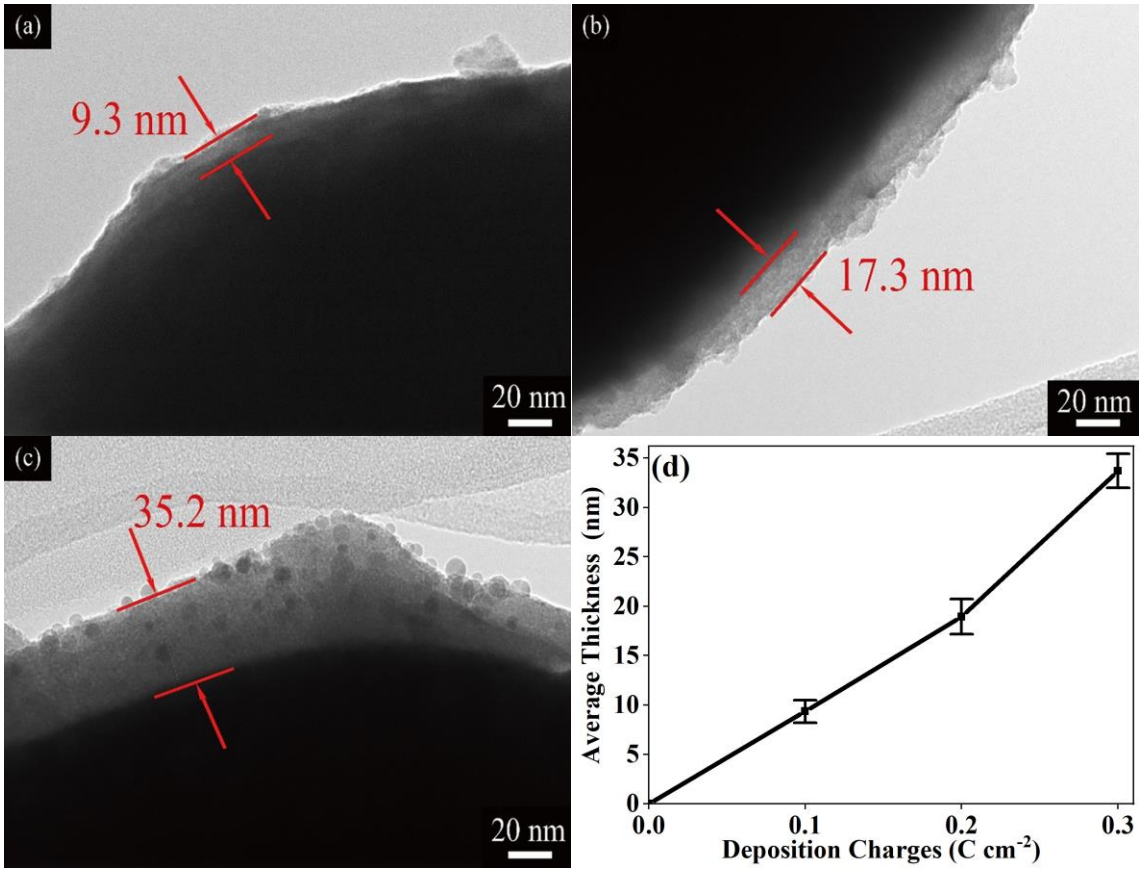

Figure S10. TEM images of the $CuBi_2O_4$ dendrites coated with the TiO_2 protective layers with different thickness. The TiO_2 protective layers were prepared by electrodeposition with controlled deposition charges: (a) 0.10 C cm^{-2}, (b) 0.20 C cm^{-2} and (c) 0.30 C cm^{-2}. (d) Dependence of the average thickness of TiO_2 protection layer on the deposition charges.

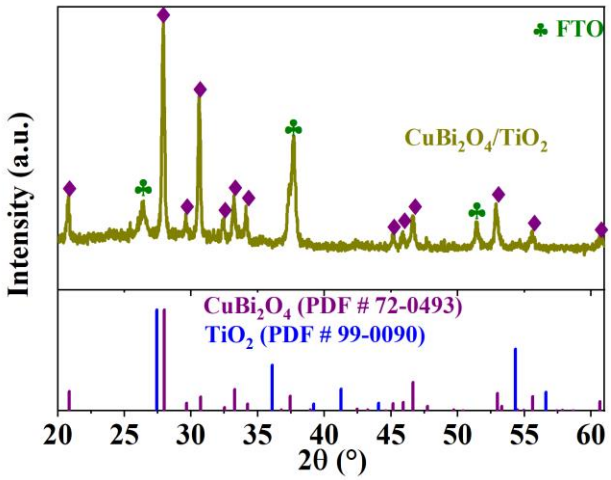

Figure S11. The XRD pattern of the dendritic $CuBi_2O_4/TiO_2$ film prepared on FTO substrate.

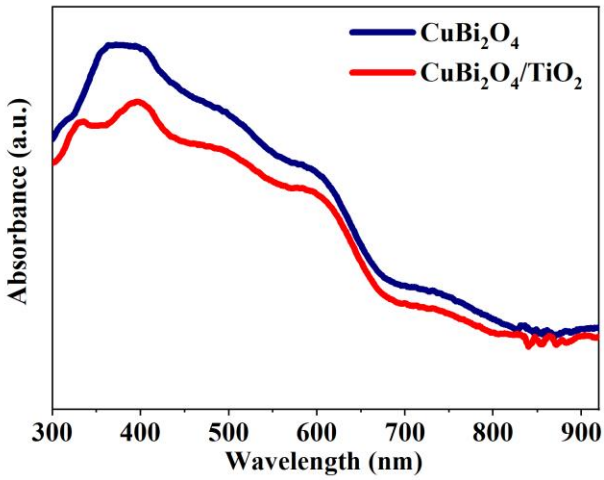

Figure S12. UV-vis absorption spectra of the bare $CuBi_2O_4$ and the $CuBi_2O_4/TiO_2$ dendrites.

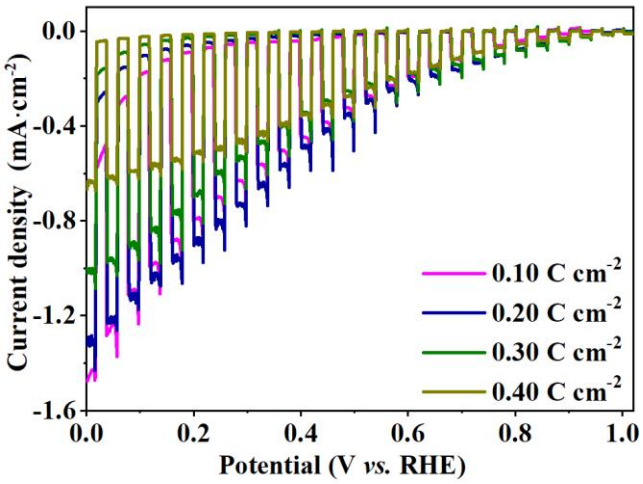

Figure S13. Effect of the different thicknesses of TiO_2 overlayer determined by passing charges on PEC photoactivity in 0.10 M Na_2SO_4 of its corresponding composite photocathode.

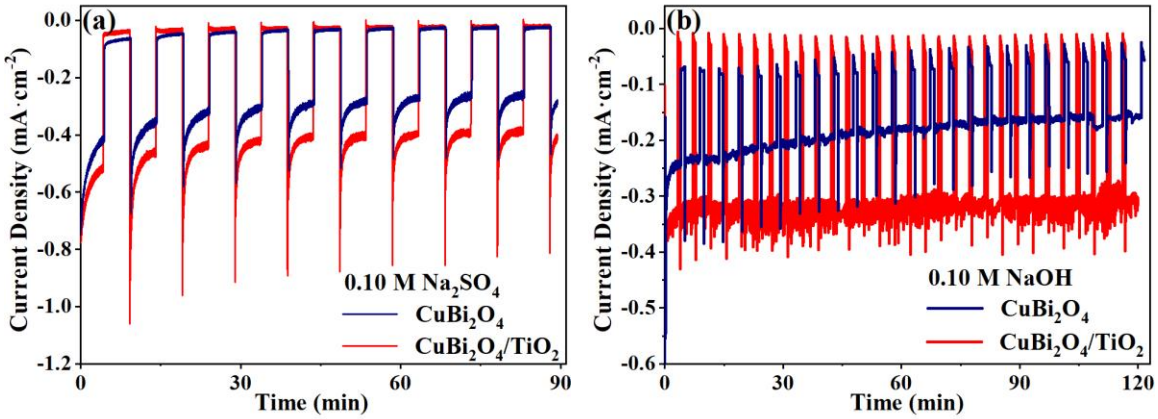

Figure S14. (a) at 0.400 V *vs*. RHE in 0.10 M Na_2SO_4 and (b) at 0.600 V *vs*. RHE in 0.10 M NaOH under chopped illumination (100.0 mW cm^{-2}). The TiO_2 protective layer was prepared by electrodeposition with the deposition charge of 0.20 C cm^{-2}.

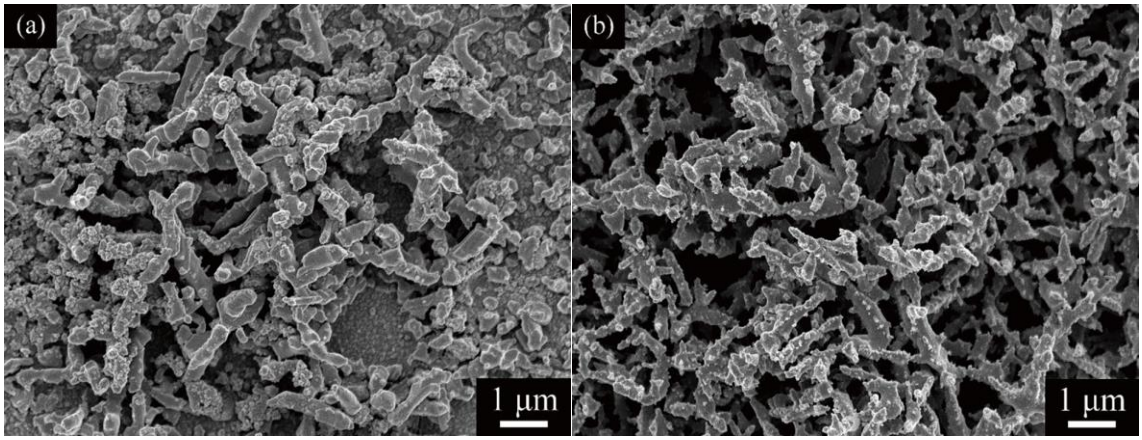

Figure S15. Typical top-view SEM images of (a) the bare $CuBi_2O_4$ and (b) the $CuBi_2O_4/TiO_2$ after stability measurements.

Table S1. Photocurrent density (J_{ph}) at required potential of the $CuBi_2O_4$ based photocathodes for HER in neutral electrolyte reported in literature.

Photocathode	Morphology	Electrolyte	pH	J_{ph} [mA cm^{-2}] at 0.2 V *vs.* RHE	Ref.
$CuBi_2O_4$	Dendrites	0.10 M Na_2SO_4	6.8	0.83	This work
$CuBi_2O_4/TiO_2$	Dendrites	0.10 M Na_2SO_4,	6.8	0.90	This work
Au/ $CuBi_2O_4$/Pt	Polyhedral shape	0.1 M Na_2SO_4,	6.8	1.00	[2]
$CuBi_2O_4$/ZnS/TiO_2	Porous film	0.3 M K_2SO_4+0.2 M PBS	6.65	0.60	[3]
CuO/$CuBi_2O_4$	Flower shape	0.1 M Na_2SO_4,	6.8	0.60	[4]
$CuBi_2O_4$/Au/carbon nanosheet	Porous film	0.1 M K_2SO_4+0.2 M PBS	6.68	0.52	[5]
$CuBi_2O_4$/Polythiophene	Porous film	0.3 M K_2SO_4 +0.2 M PBS	6.66	0.51	[6]
$CuBi_2O_4/BiVO_4$	Porous film	0.1 M Na_2SO_4	6	0.48	[7]
$CuBi_2O_4$	Nanotextured film	0.1 M Na_2SO_4,	6.8	0.46	[8]
CuO/$CuBi_2O_4$	Irregular shape	0.1 M Na_2SO_4,	6.8	0.30	[9]
$CuBi_2O_4$/rGO	Irregular shape	0.5 M Na_2SO_4,	6.8	0.25	[10]
CuO/$CuBi_2O_4$/Pt	Irregular shape	0.3 M K_2SO_4+0.1 M PBS	6.8	0.24	[11]

$CuBi_2O_4$/Ag,N co-doped graphene quantum dots	Submicron rods	0.5 M Na_2SO_4	6.6	0.08	[12]

(1) PBS represents phosphate buffer solution.

Table S2. Photocurrent density (J_{ph}) at required potential of the $CuBi_2O_4$ based photocathodes for HER in neutral electrolyte with electron scavenger reported in literature.

Photocathode	Morphology	Electrolyte	Electron scavenger	pH	J_{ph} [mA cm^{-2}] at 0.6 V *vs*. RHE	Ref.
$CuBi_2O_4$	Dendrites	0.10 M Na_2SO_4	H_2O_2	6.8	3.21	This work
Cu doped NiO/ $CuBi_2O_4$	Planar film	0.3 M K_2SO_4+0.2 M PBS	H_2O_2	6.65	2.83	[13]
$CuBi_2O_4$	Porous film	0.3 M K_2SO_4+0.2 M PBS	H_2O_2	6.65	2.66	[14]
Gradient $CuBi_2O_4$/CdS/TiO_2/Pt	Planar film	0.3 M K_2SO_4+0.2 M PBS	H_2O_2	6.65	2.50	[15]
$CuBi_2O_4$	Planar film	0.2 M K_2SO_4+0.1 M PBS	H_2O_2	6.8	2.30	[16]
$CuBi_2O_4$ (Bi:Cu=1.5)	Planar film	0.1 M $KHCO_3$	$Na_2S_2O_8$	8.2	1.21	[17]
$CuBi_2O_4$/$Cu_{1.5}TiO_z$	Planar film	0.1 M $KHCO_3$	$Na_2S_2O_8$	8.2	1.40	[18]

(1) PBS represents phosphate buffer solution.

REFERENCES

(1) Zhang, X.; Sun, X.; Guo, S.-X.; Bond, A. M.; Zhang, J., Formation of Lattice-Dislocated Bismuth Nanowires on Copper Foam for Enhanced Electrocatalytic CO_2 Reduction at Low Overpotential. *Energy Environ. Sci.* **2019**, *12*, 1334-1340.

(2) Cao, D.; Nasori, N.; Wang, Z.; Mi, Y.; Wen, L.; Yang, Y.; Qu, S.; Wang, Z.; Lei, Y., p-Type $CuBi_2O_4$: An Easily Accessible Photocathodic Material for High-Efficiency Water Splitting. *J. Mater. Chem. A* **2016**, *4*, 8995-9001.

(3) Wei, S.; Xu, N.; Li, F.; Long, X.; Hu, Y.; Gao, L.; Wang, C.; Li, S.; Ma, J.; Jin, J., Rationally Designed Heterojunction on a $CuBi_2O_4$ Photocathode for Improved Activity and Stability During Photoelectrochemical Water Reduction. *ChemElectroChem* **2019**, *6*, 3367-3374.

(4) Patil, R.; Kelkar, S.; Naphade, R.; Ogale, S., Low Temperature Grown $CuBi_2O_4$ with Flower Morphology and Its Composite with CuO Nanosheets for Photoelectrochemical Water Splitting. *J. Mater. Chem. A* **2014**, *2*, 3661-3668.

(5) Xu, N.; Li, F.; Gao, L.; Hu, H.; Hu, Y.; Long, X.; Ma, J.; Jin, J., N,Cu-Codoped Carbon Nanosheet/Au/$CuBi_2O_4$ Photocathodes for Efficient Photoelectrochemical Water Splitting. *ACS Sustainable Chem. Eng.* **2018**, *6*, 7257-7264.

(6) Xu, N.; Li, F.; Gao, L.; Hu, H.; Hu, Y.; Long, X.; Ma, J.; Jin, J., Polythiophene Coated $CuBi_2O_4$ Networks: A Porous Inorganic–Organic Hybrid Heterostructure for Enhanced Photoelectrochemical Hydrogen Evolution. *Int. J. Hydrogen Energy* **2018**, *43*, 2064-2072.

(7) Liu, S.; Zhou, J.; Lu, Y.; Su, J., Pulsed Laser/Electrodeposited $CuBi_2O_4/BiVO_4$ Pn Heterojunction for Solar Water Splitting. *Sol. Energy Mater. Sol. Cells* **2018**, *180*, 123-129.

(8) Li, J.; Griep, M.; Choi, Y.; Chu, D., Photoelectrochemical Overall Water Splitting with Textured $CuBi_2O_4$ as a Photocathode. *Chem. Commun.* **2018**, *54*, 3331-3334.

(9) Hossain, M. K.; Samu, G. F.; Gandha, K.; Santhanagopalan, S.; Liu, J. P.; Janáky, C.; Rajeshwar, K., Solution Combustion Synthesis, Characterization, and Photocatalytic Activity of $CuBi_2O_4$ and Its Nanocomposites with CuO and α-Bi_2O_3. *J. Phys. Chem. C* **2017**, *121*, 8252-8261.

(10) Shah, A. K.; Sahu, T. K.; Banik, A.; Gogoi, D.; Peela, N. R.; Qureshi, M., Reduced Graphene Oxide Modified $CuBi_2O_4$ as an Efficient and Noble Metal Free Photocathode for Superior Photoelectrochemical Hydrogen Production. *Sustainable Energy Fuels* **2019**, *3*, 1554-1561.

(11) Park, H. S.; Lee, C.-Y.; Reisner, E., Photoelectrochemical Reduction of Aqueous Protons with a CuO|$CuBi_2O_4$ Heterojunction under Visible Light Irradiation. *Phys. Chem. Chem. Phys.* **2014**, *16*, 22462-22465.

(12) Ma, C.; Ma, D.-K.; Yu, W.; Chen, W.; Huang, S., Ag and N-Doped Graphene Quantum Dots Co-Modified $CuBi_2O_4$ Submicron Rod Photocathodes with Enhanced Photoelectrochemical Activity. *Appl. Surf. Sci.* **2019**, *481*, 661-668.

(13) Song, A.; Plate, P.; Chemseddine, A.; Wang, F.; Abdi, F. F.; Wollgarten, M.; van de Krol, R.; Berglund, S. P., Cu:NiO as a Hole-Selective Back Contact to Improve the

Photoelectrochemical Performance of $CuBi_2O_4$ Thin Film Photocathodes. *J. Mater. Chem. A* **2019**, *7*, 9183-9194.

(14) Xu, Y.; Jian, J.; Li, F.; Liu, W.; Jia, L.; Wang, H., Porous $CuBi_2O_4$ Photocathodes with Rationally Engineered Morphology and Composition Towards High-Efficiency Photoelectrochemical Performance. *J. Mater. Chem. A* **2019**, *7*, 21997-22004.

(15) Wang, F.; Septina, W.; Chemseddine, A.; Abdi, F. F.; Friedrich, D.; Bogdanoff, P.; van de Krol, R.; Tilley, S. D.; Berglund, S. P., Gradient Self-Doped $CuBi_2O_4$ with Highly Improved Charge Separation Efficiency. *J. Am. Chem. Soc.* **2017**, *139*, 15094-15103.

(16) Oropeza, F. E.; Feleki, B. T.; Zhang, K. H.; Hensen, E. J.; Hofmann, J. P., Influence of Reduced Cu Surface States on the Photoelectrochemical Properties of $CuBi_2O_4$. *ACS Appl. Energy Mater.* **2019**, *2*, 6866-6874.

(17) Zhang, Z.; Lindley, S. A.; Dhall, R.; Bustillo, K.; Han, W.; Xie, E.; Cooper, J. K., Beneficial CuO Phase Segregation in the Ternary P-Type Oxide Photocathode $CuBi_2O_4$. *ACS Appl. Energy Mater.* **2019**, *2*, 4111-4117.

(18) Zhang, Z.; Lindley, S. A.; Guevarra, D.; Kan, K.; Shinde, A.; Gregoire, J. M.; Han, W.; Xie, E.; Haber, J. A.; Cooper, J. K., Fermi Level Engineering of Passivation and Electron Transport Materials for p-Type $CuBi_2O_4$ Employing a High-Throughput Methodology. *Adv. Funct. Mater.* **2020**, *30*, 2000948.